atmosphere

MDPI

Article

Cloud Radar Observations of Diurnal and Seasonal Cloudiness over Reunion Island

Jonathan Durand [1], Edouard Lees [1], Olivier Bousquet [1,2,*], Julien Delanoë [3] and François Bonnardot [4]

[1] Laboratoire de l'Atmosphère et des Cyclones (UMR8105 LACy), Université de La Réunion, CNRS, Météo-France, 97400 Saint-Denis, France; jonathan.durand@univ-reunion.fr (J.D.); edouard.lees@meteo.fr (E.L.)
[2] Institute for Coastal Marine Research (CMR), Nelson Mandela University, Port-Elizabeth 6001, South Africa
[3] Laboratoire Atmosphère, Milieux et Observations Spatiales (UMR 8190 LATMOS), CNRS/Sorbonne Université/USVQ, 78280 Guyancourt, France; Julien.Delanoe@latmos.ipsl.fr
[4] Direction Interrégionale de Météo-France pour l'Océan Indien, Saint-Denis, 97490 Sainte-Clotilde, France; francois.bonnardot@meteo.fr
* Correspondence: olivier.bousquet@meteo.fr

Abstract: In November 2016, a 95 GHz cloud radar was permanently deployed in Reunion Island to investigate the vertical distribution of tropical clouds and monitor the temporal variability of cloudiness in the frame of the pan-European research infrastructure Aerosol, Clouds and Trace gases Research InfraStructure (ACTRIS). In the present study, reflectivity observations collected during the two first years of operation (2016–2018) of this vertically pointing cloud radar are relied upon to investigate the diurnal and seasonal cycle of cloudiness in the northern part of this island. During the wet season (December–March), cloudiness is particularly pronounced between 1–3 km above sea level (with a frequency of cloud occurrence of 45% between 12:00–19:00 LST) and 8–12 km (with a frequency of cloud occurrence of 15% between 14:00–19:00 LST). During the dry season (June–September), this bimodal vertical mode is no longer observed and the vertical cloud extension is essentially limited to a height of 3 km due to both the drop-in humidity resulting from the northward migration of the ITCZ and the capping effect of the trade winds inversion. The frequency of cloud occurrence is at its maximum between 13:00–18:00 LST, with a probability of 35% at 15 LST near an altitude of 2 km. The analysis of global navigation satellite system (GNSS)-derived weather data also shows that the diurnal cycle of low- (1–3 km) and mid-to-high level (5–10 km) clouds is strongly correlated with the diurnal evolution of tropospheric humidity, suggesting that additional moisture is advected towards the island by the sea breeze regime. The detailed analysis of cloudiness observations collected during the four seasons sampled in 2017 and 2018 also shows substantial differences between the two years, possibly associated with a strong positive Indian Ocean Southern Dipole (IOSD) event extending throughout the year 2017.

Keywords: cloud radar; BASTA; Indian Ocean Subtropical Dipole; Reunion Island; integrated water vapor; Southwest Indian Ocean; GNSS; cloudiness variability; tropical clouds

Citation: Durand, J.; Lees, E.; Bousquet, O.; Delanoë, J.; Bonnardot, F. Cloud Radar Observations of Diurnal and Seasonal Cloudiness over Reunion Island. *Atmosphere* **2021**, *12*, 868. https://doi.org/10.3390/atmos12070868

Academic Editors: Lawrence D. Carey and Filomena Romano

Received: 29 May 2021
Accepted: 29 June 2021
Published: 3 July 2021

Publisher's Note: MDPI stays neutral with regard to jurisdictional claims in published maps and institutional affiliations.

1. Introduction

Because cloudiness plays a major role in distributing the radiative energy available in the atmosphere [1,2], knowledge of cloud properties is crucial for anticipating the impacts of cloud cover and, in particular, low-level cloud feedbacks in climate change projections [3]. A better knowledge of the vertical distribution of clouds is also important for numerical modelling, as errors in the location and vertical structure of clouds, which directly impact the radiative balance, are considered among the main sources of uncertainty in climate and weather numerical weather prediction (NWP) models [4–6].

In the tropics, cloudiness is principally determined by the space–time distribution of the lower-tropospheric moisture, which controls the total water content and buoyancy of

atmospheric parcels. Humidity is essentially driven by the seasonal migration of the Inter-Tropical Convergence Zone (ITCZ), and its associated circulation shifts, as well as by large scale anomalies that influence atmospheric circulation at both intra-seasonal (Madden–Julian Oscillation [7,8]), and interannual (e.g., El Nino Southern Oscillation, Indian Ocean Dipole, Indian Ocean Subtropical Dipole) timescales.

Thanks to their ability to cover vast areas of the globe, spaceborne cloud radars (e.g., CloudSat) have significantly improved our understanding of the spatio-temporal distribution of clouds throughout the planet and are widely considered as one of the most efficient tools to study cloud properties at the global scale [9]. These space-borne observations are nevertheless subject to some limitations, especially at low-level, due to ground (or sea) clutter echoes [10–12] and difficulties to penetrate thick mid-level clouds to observe the low cloud beneath (due to their short wavelength). In this regard, ground-based cloud radars, which feature higher spatio-temporal time resolution than space-borne sensors, are essential to complete (and evaluate) space-borne observations, especially at the local scale [13]. Relatively few studies have however been conducted so far to investigate tropical cloud properties from ground-based cloud radars. Moreover, if one except a few studies conducted from the Atmospheric Radiation Measurement (ARM) Tropical Western Pacific (TWP) sites [14–16], the latter were essentially conducted in the northern hemisphere due to the overall lack of observation facilities available south of the equator. This includes measurements conducted in Niger [17], in the Indian Western Ghats [18], or from the Barbados Cloud Observatory (BCO [19]) to investigate the seasonality and vertical distribution of low-level clouds [20,21]. This lack of observations was further exacerbated in the last few years following the dismantling, in 2013 (Nauru) and 2014 (Darwin and Manus) of the three permanent Pacific ARM TWP sites [22]. As a consequence, the Atmospheric Physics Observatory (OPAR) of Reunion Island, a small (2512 km^2) volcanic French overseas territory located in the Southwest Indian Ocean (SWIO), has now become the principal atmospheric research facility in the southern hemisphere.

Due to its location, located both at the edge of the subtropical jet and in the subsidence region of the southern hemisphere Hadley cell, Reunion Island (20.8° S, 55.5° E) is particularly well suited to study tropical and subtropical influences on the general circulation. For this reason, OPAR's instrumentation is principally designed to observe high troposphere—low stratosphere interactions from a unique ensemble of lidars and radiometric sensors deployed at the high-altitude Maïdo observatory [23]. In order to extend cloud and precipitation observation capabilities, a new coastal experimental site was, however, recently integrated to OPAR in the frame of the pan-European research infrastructure "Aerosol, Clouds and Trace gases Research InfraStructure" (ACTRIS, https://www.actris.eu, accessed on 1 July 2021), a programme aiming at collecting high-quality observation data to constrain predictive models and improve global forecasts of the atmosphere. This new observation facility, located on the northern coast of the island at Saint-Denis de La Réunion (Figure 1), was notably equipped, in 2016, with a 95 GHz radar BASTA (Bistatic rAdar SysTem for Atmospheric Studies; [24]) to collect cloud observations at high spatial and temporal resolutions. This new site is, in particular, well-adapted to investigate coastal tropical clouds, which are known to occur over different mid-tropospheric conditions than over the open ocean and continental areas due to the combined effects of land–sea breeze interactions [25].

In this study, reflectivity observations collected during the two first years of operation of the cloud radar BASTA are used to investigate the characteristics of cloudiness in Reunion Island as well as its relationship with local and regional tropospheric humidity patterns inferred from radiosounding, Global Navigation Satellite System (GNSS) and high-resolution reanalysis data. Although limited in time, the 2-y cloud radar dataset used in this study allows us to investigate, for the first time in the SWIO, the vertical cloud properties over a remote and climatologically important location of the Southern Hemisphere, which was identified as a key component in the climate system by ACTRIS research infrastructure.

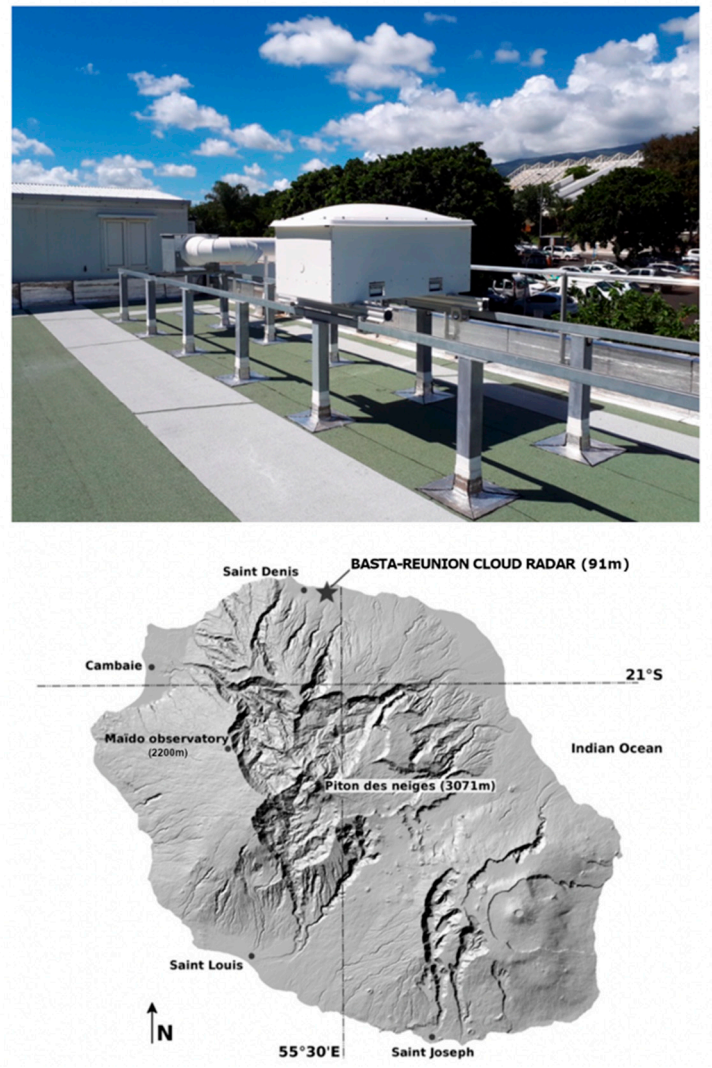

Figure 1. The cloud radar BASTA-REUNION located in Saint-Denis de La Réunion on the rooftop of Reunion University (55.48° E, 20.9° S).

This paper is organized as follows: information about data used in this study are given in Section 2; the distribution and analysis of the seasonal cloud cover over Saint-Denis between November 2016 and October 2018 are presented in Section 3; possible relationships between observed cloud patterns and large-scale environment are thus investigated in Section 4, while Section 5 presents our conclusions and perspectives.

2. Data and Methods

2.1. Cloud Radar Observations

The present study is principally based on continuous observations collected between November 2016 and October 2018 by a cloud radar BASTA. BASTA is a 95 GHz vertically pointing bistatic Doppler radar (distinct antennas for transmission and reception) developed by LATMOS ("Laboratoire Atmosphère, Milieux et Observations Spatiales") for cloud and fog studies [24,26]. A dedicated version of this radar (referred to as BASTA-REUNION) was deployed in Reunion Island in November 2016 at the main campus facility of Reunion University, located in Saint-Denis approximately 100 m above ground level (Figure 1). BASTA-REUNION provides times series of vertical reflectivity and Doppler velocity profiles up to an altitude of 24 km. Reflectivity profiles consist of a combination of data collected in four distinct operating modes that are each activated over a period of integration of 3 s and later recombined to reconstruct the cloud structure throughout the

tropospheric layer every 12 s. The first operating mode, dedicated to fog and low cloud observations, runs at the resolution of 12.5 m and provides information up to an altitude of 12 km. The second mode, which features a vertical resolution of 25 m, is used to investigate mid-level clouds between 6 km and 18 km. Finally, the last two modes (100 m vertical resolution) are used to sample high-level clouds up to 18 km and 24 km, respectively—the latter mode, which is slightly more sensitive, was specifically implemented for tropical regions. Nearly four million reconstructed vertical reflectivity profiles are used in this study, which represent ~80% of the total number of profiles theoretically expected over a 2-year period.

Due to its operating frequency, BASTA-REUNION can be strongly affected by radar attenuation resulting from the absorption or reflection of transmitted signals in precipitation areas. This phenomenon, which occurs at most radar frequencies, reflects the fact that some of the energy is often lost to scattering and absorption when the radar pulse penetrates in heavy precipitation areas. At 95 GHz, the frequency of BASTA-REUNION, uncertainties can be introduced in the observed cloud properties and occasionally can result in the extinction of the radar signal in a heavy precipitation regime. As will be seen later, this phenomenon nevertheless remains relatively uncommon in the Saint-Denis area and does not significantly affect the statistical analysis of cloud radar data that will be presented hereafter. We thus chose to not discriminate between precipitating and non-precipitating clouds so as to be able to also identify the occurrence of rainfall in radar observations—as fog and low-level stratus never occur over Saint-Denis, radar data collected below 1 km always reflect the presence of precipitation.

During the austral summer, the presence of the Intertropical Convergence Zone (ITCZ) nearby Reunion Island induces low-level convergence of highly buoyant air that favors the development of deep convection. The interactions of these unstable air masses with the complex orography of the island can generate very intense precipitation due, in particular, to the passage of tropical cyclones nearby [27]. In winter, as the ITCZ moves back northwards, the local weather becomes mostly influenced by the subsided southern branch of the Hadley cell. The resulting temperature inversion tends to inhibit atmospheric upward vertical motion above ~3 km [28,29] and is further amplified by the trade wind inversion [30–32]. Due to its complex orography, Reunion Island is also affected all year long by thermally induced sea breeze circulations that can force onshore moist flow at low levels and further favors the development of low-level clouds during daytime [30,33]. Examples of observations collected by BASTA-REUNION in Austral summer (26 March 2017), Austral winter (1 August 2017) as well as during cyclonic conditions (4–6 March 2018) are presented hereafter to illustrate the general cloudiness conditions associated with the various large-scale circulation patterns that drive cloud formation in Reunion Island.

In Austral summer (Figure 2a, 26 March 2017), radar observations show the existence of a strong diurnal cycle characterized by low-level clouds forming early in the morning and eventually dissipating in the late evening. Convective clouds, resulting from the high convective instability that prevails over the tropical SWIO basin during summer, develop in the early afternoon and extend up to the altitude of 10 km (all heights are given above mean sea level). Precipitation, as evidenced by associated time series of collocated rain gauge measurements, is maximised around mid-day (9–11 UTC, 13–15 LST) and dissipates in the early evening. During winter (Figure 2b, 1 August 2017), low-level clouds also form in the early morning (near 03:00 UTC/07:00 LST), but never evolve into deep convective clouds due to the strong capping effect. These low-level clouds, which consist of small, non-precipitating, scattered cumulus, are not advected from the ocean, but develop over the slopes before expanding northwards towards the coast in the middle of the afternoon.

The third example (Figure 3) shows radar observations collected during the passage of tropical cyclone Dumazile over the Mascarene Archipelago in early March 2018. On 4 March (top panel), radar observations were collected within an outer rainband located about 700 km southeast of the TC center. Time series of vertical radar reflectivity profiles show numerous convective cells extending forward and backward up to an altitude of

15 km. On 6 March (bottom panel), radar data are collected within a cirriform region, at the back of the tropical cyclone. Vertical reflectivity profiles collected in this area (indicated by the red circle on the associated MODIS image) show a layer of cirrus clouds extending from 11 to 14 km that is characteristic of pre- and post-convective tropical cyclone regions. As shown by collocated high-resolution (6 min) rainfall measurements, brief but extremely strong rainfall occurred on 4 March around 09:00 UTC (up to 50 mmh^{-1}) and 10:15 UTC (up to 95 mmh^{-1}). These heavy precipitation periods are associated with data gaps in radar observations, which can also be observed in Figure 2a (between 8 and 11 UTC). These gaps reflect the aforementioned attenuation of the radar signal by strong precipitation, which principally occurs for instantaneous rain rates higher than 15 mm h^{-1} (Figures 2a and 3). According to the climatological study of [31], which provides a detailed analysis of the spatio-temporal variability of local rainfall patterns over Reunion Island, such situations are nevertheless uncommon in the Saint-Denis area, and not frequent enough to significantly impact the results that will be presented in the following.

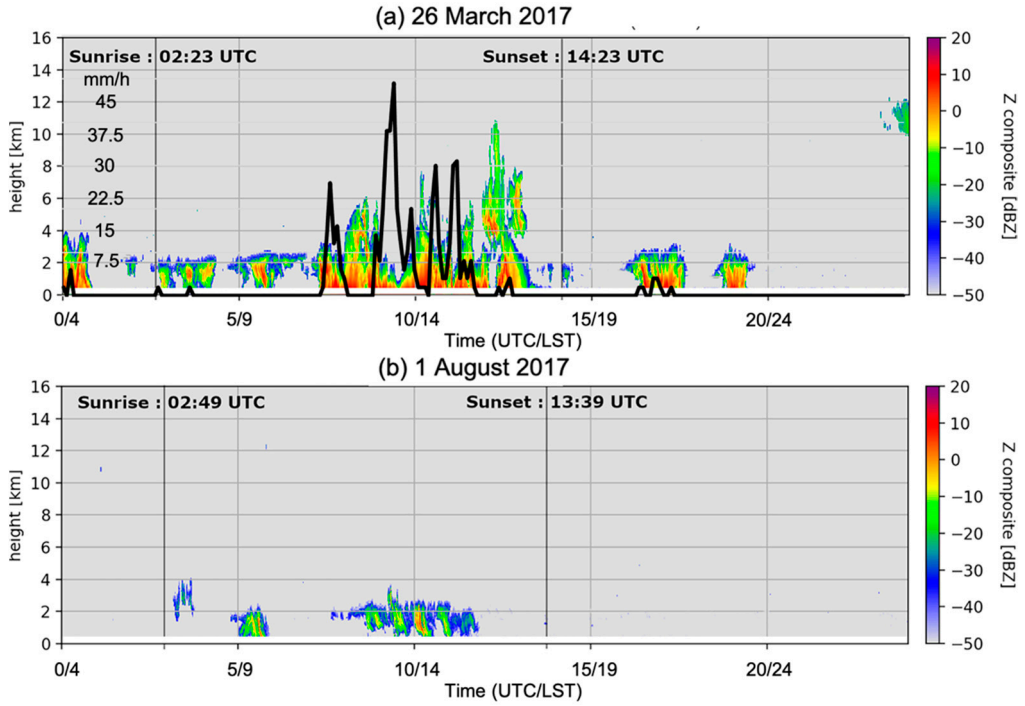

Figure 2. Time series of radar reflectivity vertical profiles (dBZ) collected on (**a**) 26 March 2017 (summer) and (**b**) 1 August 2017 (winter). The black line in (**a**) shows collocated rainfall measurements every 6 min expressed in mmh^{-1} (scale to the left).

2.2. Other Datasets

Additional sources of data are also relied upon to describe the local and regional weather conditions prevailing over Reunion Island and the SWIO basin during the 2-year period of analysis:

(i) In situ observations of relative humidity inferred from Saint-Denis' airport (20.88° S, 55.51° E) operational daily radiosounding data collected between 2014 and 2018;

(ii) Time series of integrated water vapor (IWV) columns, inferred from the analysis of GNSS data collected from the IGN (Institut Geographique National) station STDE (20.88° S–55.51° E) and the International GNSS System (IGS)' station REUN (21.2° S, 55.57° E). GNSS data are processed following the approach used by [34,35] to produce IWV data at various locations in the SWIO basin (a complete description of GNSS IWV retrieval and associated uncertainties can be found in the former papers).

(iii) Reanalysis data extracted from European Center for Medium-Range Weather Forecast (ECMWF)'s 5th generation reanalysis (ERA5) are used to investigate the regional atmospheric conditions prevailing over the SWIO basin. ERA5 provides hourly estimates of numerous atmospheric, land and oceanic climate variables on a 0.25 × 0.25° horizontal grid [36]. Reanalysis data used in this study consist of wind, humidity, sea level pressure and vertical velocity fields extracted over the period 1990–2020.

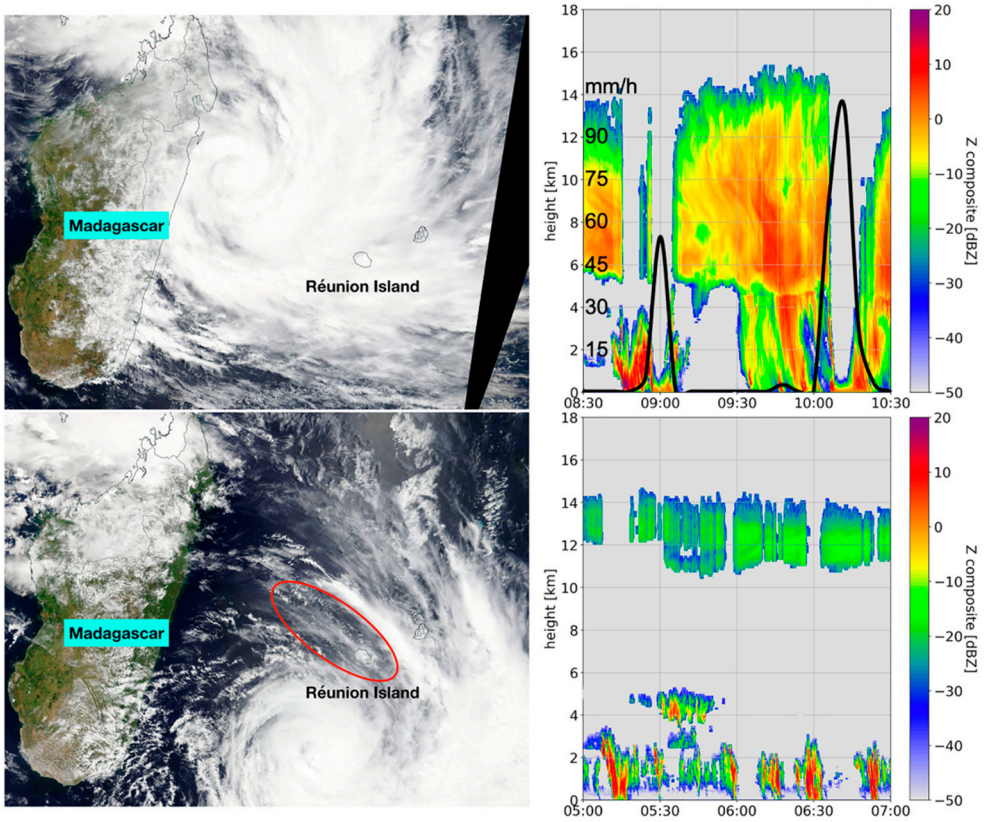

Figure 3. Left panel: Satellite images (MODIS TERRA) of Tropical Cyclone Dumazile, recorded on 4 March 2018 (**top**, 9:00 UTC) and 6 March 2018 (**bottom**, 6:00 UTC). Right panel: corresponding time series of BASTA-REUNION vertical radar reflectivity profiles (dBZ, UTC) with superimposed collocated rainfall measurements every 6 min (expressed in mmh^{-1}, scale to the left). The red circle indicates the cirriform region sampled by the radar on 6 March.

3. Diurnal and Seasonal Variability of Cloudiness over Saint-Denis in 2017 and 2018

In the following, reflectivity data collected by BASTA-REUNION are used to investigate the vertical structure of winter and summer clouds over Saint-Denis. For simplicity, the four seasons investigated hereafter will be referred to as summer 2017 (November 2016–March 2017), winter 2017 (June–September 2017), summer 2018 (November 2017–March 2018) and winter 2018 (June–September 2018).

Diurnal Cycle

The seasonal composite analyses of radar reflectivity profiles aggregated over the two sampled summer and the two winter seasons are shown in Figure 4a,b, respectively.

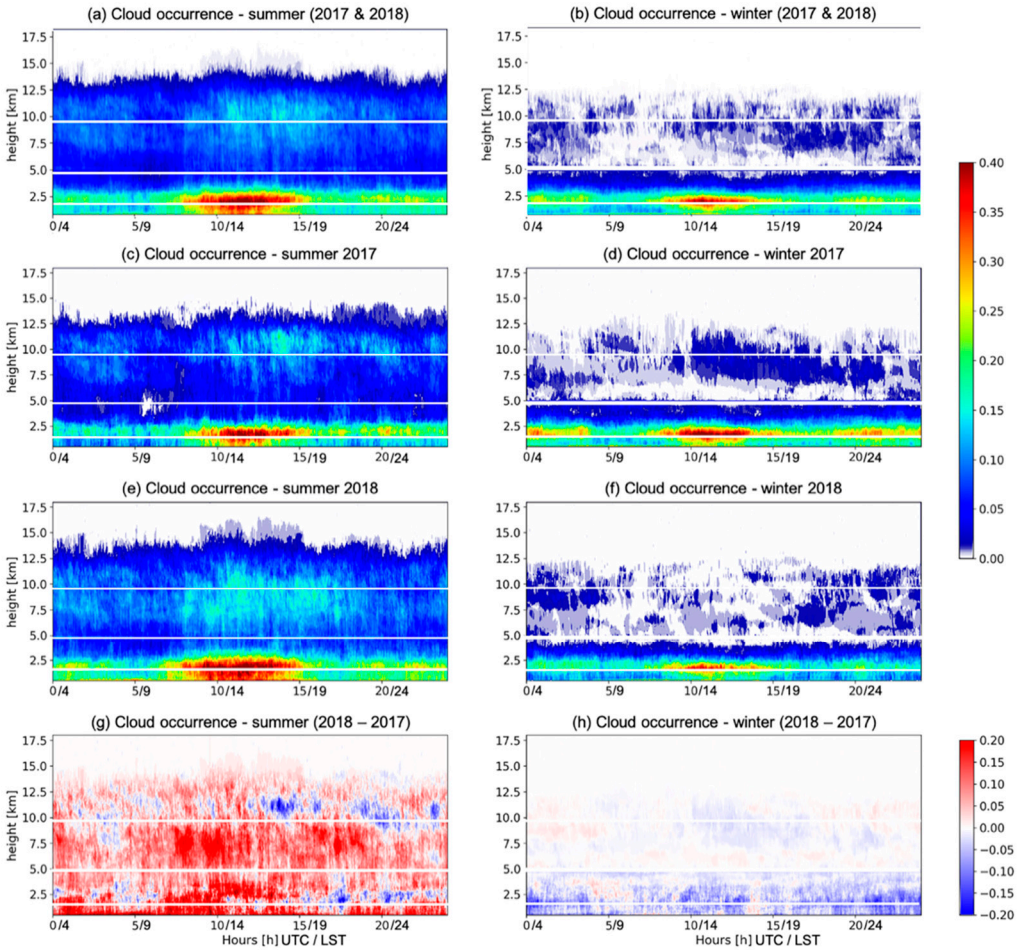

Figure 4. Time series of cloud occurrence (%, normalized to 1) as a function of the time of the day (hours) and altitude (km) for (**a**) aggregated summer seasons 2017 and 2018, (**b**) aggregated winter seasons 2017 and 2018, (**c**) summer 2017, (**d**) winter 2017, (**e**) summer 2018, (**f**) winter 2018, (**g**) summer 2018 minus summer 2017 and (**h**) winter 2018 minus winter 2017. White lines near the altitudes 2, 5 and 10 km correspond to data gap layers of ~25–50 m resulting from the recombination of data collected in the different radar acquisition modes.

In summer (Figure 4a), aggregated radar observations show two cloud layers, associated with the diurnal cycle (leading to the formation of low-level cumulus clouds) and convective instability (leading to the development of thunderstorm systems in mid to late afternoon). In the lowest layer, which extends from ~0.5 to 3 km, the maximum cloud occurrence is observed between 08:00 UTC (12 LST) and 15:00 UTC (19 LST) at an altitude of 2 km, with a maximum probability of nearly 45% near 12 UTC (16 LST). The upper layer, comprised between ~6 and 15 km, corresponds to deep convective and ice clouds associated with local storms, as well as tropical storms and cyclones that passed nearby Reunion Island. The probability of occurrence is maximised between 10:00 UTC and 15:00 UTC (14–19 LST) and reaches up to 15% at an altitude of 10 km near 14 UTC (18 LST).

In winter (Figure 4b), one can still observe a layer of low-level clouds extending from approximately 0.5 to 2.5 km. The frequency of cloud occurrence is highest between 09:00 UTC (13 LST) and 14:00 UTC (18 LST), with a maximum probability of about 35% near 2km altitude at 11 UTC (15 LST). While the frequency of occurrence of low-level clouds appears similar during summer and winter periods, the depth of the low-level cloud layer is lower in winter (maximum height of 2.5 km vs. 3 km in summer). High-level clouds are also up to three times less frequent in winter (5% occurrence vs.15% occurrence in summer) as a result of the stronger stability of the atmosphere during this season.

To further assess the diurnal variability of cloud cover from one year to the next, time series shown in Figure 4a,b were also individually aggregated for each of the four sampled seasons: summer 2017 (Figure 4c) and 2018 (Figure 4e), and winter 2017 (Figure 4d) and 2018 (Figure 4f). From a qualitative standpoint, one can observe strong similarities between both summers and both winters. However, a closer look at the field of differences (Figure 4g,h) shows important disparities from one year to the next. Hence, low-level cloudiness appears significantly higher and deeper in winter 2017 (Figure 4h) than during the following winter season, while significant differences could also be observed throughout the troposphere between the two summer seasons (Figure 4g), with significantly deeper cloud cover in 2018.

Mean vertical profiles of cloud occurrence inferred from the high-resolution BASTA-REUNION profiles collected during the four sampled seasons shown in Figure 4c–f are shown in Figure 5. During summer, the probability of occurrence shows much larger values in 2018 (solid blue line) at both low-level (frequency of cloud/precipitation occurrence below 3 km ranging from 20–22% vs. 15–20% in 2017) and mid-to-high level (frequency of cloud occurrence of 10% vs. 5% in 2017 at 6 km). These differences are even more striking in winter. In 2017 (red dashed line), low-level cloudiness is for instance twice as large as in 2018 (blue-dashed line, 20–22% vs. 10%) and actually bears strong resemblances with that observed during the previous summer (solid blue line). Furthermore, one can also observe large differences occurring at mid-levels. While the vertical cloud extension is more or less limited to 4 km in 2018, in good agreement with previous climatological studies of [30,31], clouds occur in much more significant proportions up to an altitude of 6 km and even beyond (frequency of occurrence of 1% at 8 km) in 2017. In the following, large-scale environmental conditions inferred from the analysis of ERA5 data are investigated in order to understand the possible origins of these differences.

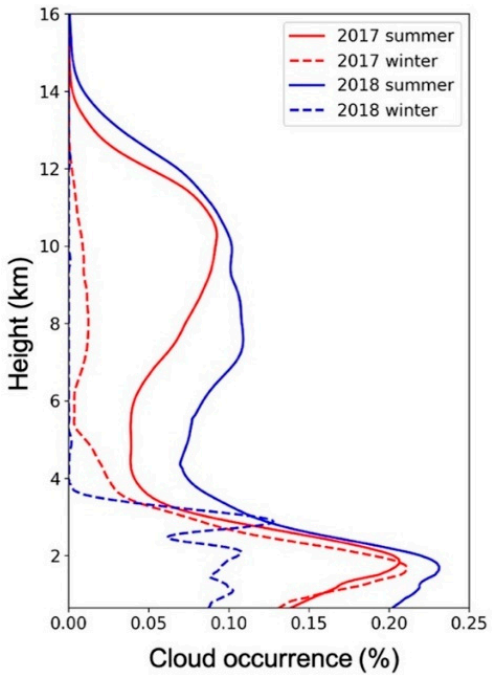

Figure 5. Probability of cloud occurrence (%, normalized to 1) observed during summer (solid line) and winter (dashed line) 2017 (red) and 2018 (blue) as a function of height.

4. Analysis of Local and Large-Scale Environmental Conditions Prevailing in 2017 and 2018

4.1. IOSD Patterns

In the SWIO basin, the main climatic phenomenon that drives large-scale oceanic and atmospheric circulation is the Indian Ocean Subtropical Dipole (IOSD [37]). This climate

anomaly controls the structure of the ocean's surface layer, which, in turn, impacts the atmospheric circulation and rainfall at the regional scale. It is characterized by three distinct phases that are defined by a reference index computed from SST anomaly differences between the western and eastern parts of the basin: a neutral phase, corresponding to the mean state of the ocean, a negative phase and a positive phase. Positive events, which are characterized by above-normal SSTs in the southwestern part of the basin and below-normal SSTs off western Australia, generally start at the beginning of the Austral summer and die off in April/May.

The evolution of the IOSD index from 2013 to 2019 (Figure 6) shows that a particularly strong positive event occurred in early 2017. The latter started in November 2016, peaked in January (with a high index value) and finally died off in late March 2017 (index value of 0.2). However, one can observe that index values started to re-increase significantly at the beginning of the winter, with an average value of ~1 throughout the rest of the year, before finally collapsing in early 2018.

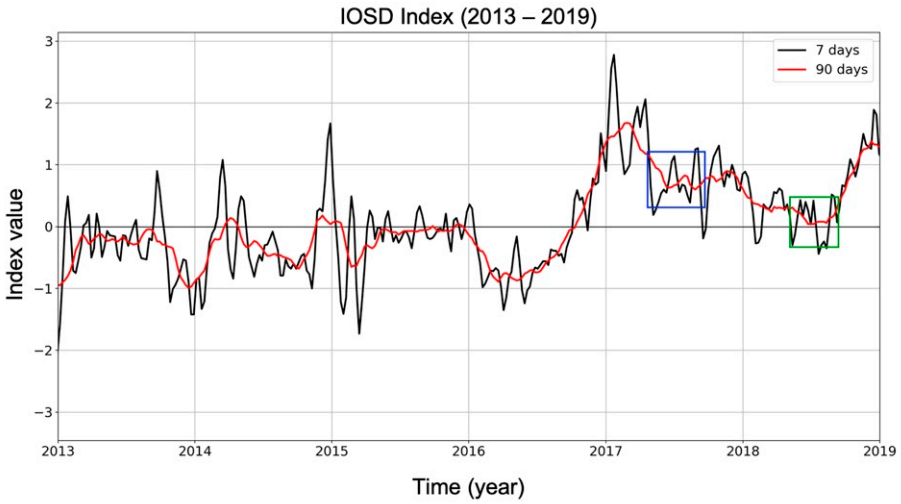

Figure 6. Averaged weekly (black) and quarterly (red) IOSD index between January 2013 and December 2019. Blue and green squares highlight index values during winter 2017 and 2018, respectively.

4.2. Large Scale Anomalies

Corresponding large-scale atmospheric and oceanic anomalies prevailing during summers (DJF) and winters (JJA) 2017 and 2018 are shown in Figures 7 and 8. In good agreement with the occurrence of a positive IOSD event, a positive SST anomaly, centered near 30° S and extending from the East African coast to ~90° E, can be observed over the SW part of the basin in summer 2017 (Figure 7a). Enhanced midlevel subsidence is also observed over Madagascar and the central part of the basin (Figure 7e), resulting in both positive pressure anomalies (Figure 7c) and dryer conditions in the mid-troposphere (as inferred from IWV anomalies, Figure 7g) in these areas. Over the Mascarenes and Reunion Island, these large-scale conditions result in a slightly positive SST anomaly, of nearly 0.5 °C, and a below-normal (negative) humidity anomaly of ~ 6–8 kg m^{-2}.

During the next summer, a positive SST anomaly can still be observed in the southern part of the basin (Figure 7b). The latter is however shifted southeastwards with respect to summer 2017 and no significant surface pressure (Figure 7d) or mid-level vertical velocity (Figure 7f) anomalies are longer observed over the central part of the basin. A moist tongue extending northwestwards towards Madagascar could be observed, in good agreement with the location of the positive SST anomaly (Figure 7h). Over the Mascarene Archipelago, these large-scale conditions resulted in positive SST and moisture anomalies of up to 1 °C and 8 kg m^{-2}, respectively.

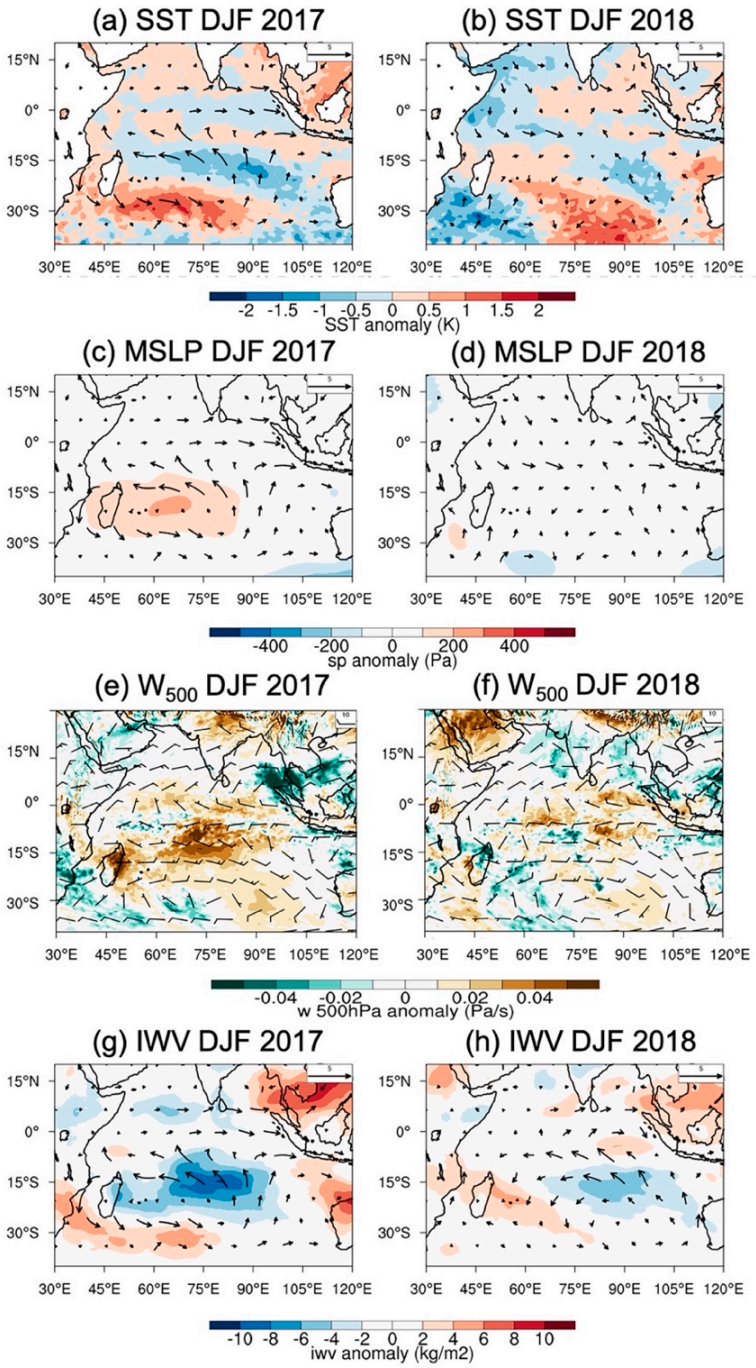

Figure 7. (**a**,**b**) Sea Surface Temperature (SST), Mean Sea Level Pressure (MSLP), Vertical velocity at 500 hPa (W) and Integrated Water Vapour (IWV) anomalies in summer (DJF) 2017 (**left panel**) and 2018 (**right panel**), computed from ERA5 reanalysis data over the period 1990–2020.

During winter 2017 (Figure 8a), ERA5 data show SST anomalies of up to 1 °C over the Mascarene Archipelago, likely inherited from the IOSD event that started earlier in the year. The Mascarene anticyclone also moved south-eastwards resulting in strong positive pressure anomalies over the central and southern parts of the basin as well as slightly below normal sea level pressures over the Mascarenes (Figure 8c). These anomalies are also accompanied by a decrease in the large-scale midlevel (500 hPa) subsidence over this area (Figure 8e), resulting in higher humidity content at 850 hPa (Figure 8g). While this positive SST anomaly is also present in winter 2018 (Figure 8b), the other atmospheric parameters (Figure 8d,f,h) are nevertheless globally in phase with the climatology.

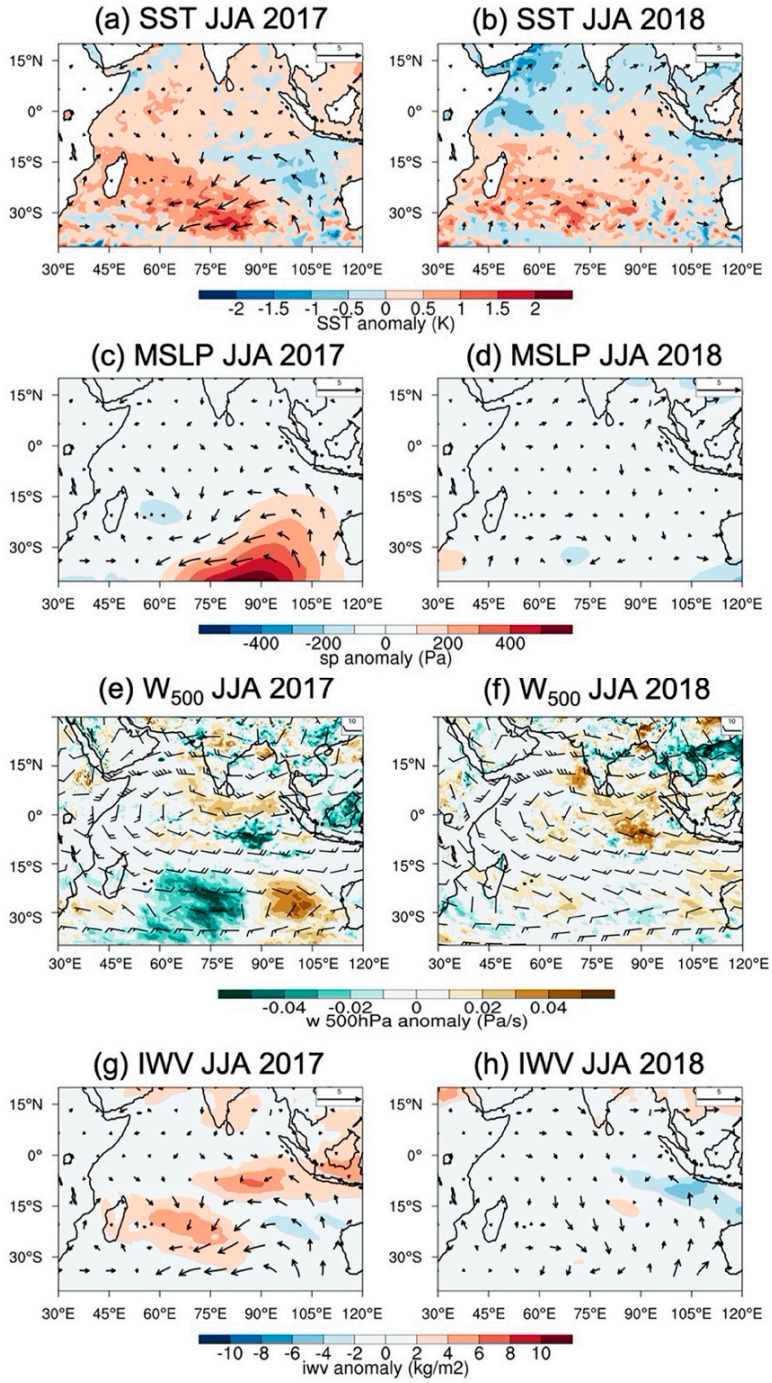

Figure 8. (**a**,**b**) Sea Surface Temperature (SST), Mean Sea Level Pressure (MSLP), Vertical velocity at 500 hPa (W) and Integrated Water Vapour (IWV) anomalies in summer (DJF) 2017 (**left panel**) and 2018 (**right panel**), computed from ERA5 reanalysis data over the period 1990–2020. As in Figure 7, but for winter (JJA) 2017 and 2018.

4.3. Local Observations

Humidity observations inferred from the analysis of GNSS data collected at the IGS station of REUN (21.2° S, 55.57° E) and radio sounding data collected at Saint-Denis' airport (20.88° S, 55.51° E) are shown in Figure 9. According to time series of monthly averaged GNSS-derived IWV columns (Figure 9a), significantly dryer conditions occurred over Reunion Island during the first 4 months (Nov–March) of the wet season 2017, with differences of up to 12 kg m^{-2} (+/−30%) compared to the same period one year after.

This tendency however inverts at the end of the summer, a period that corresponds to the dying of the 2017 positive IOSD event. GNSS-derived IWV observations also confirm that tropospheric humidity was significantly higher during winter 2017 (JJAS, blue line) than during winter 2018 (red line), with differences of up to 3.5 kg m^{-2} (+/−35%) between July and September. A strictly similar tendency (not shown) was also observed at other GNSS stations located along the west coast and central area of Reunion Island, indicating that these tropospheric humidity anomalies have impacted the whole island.

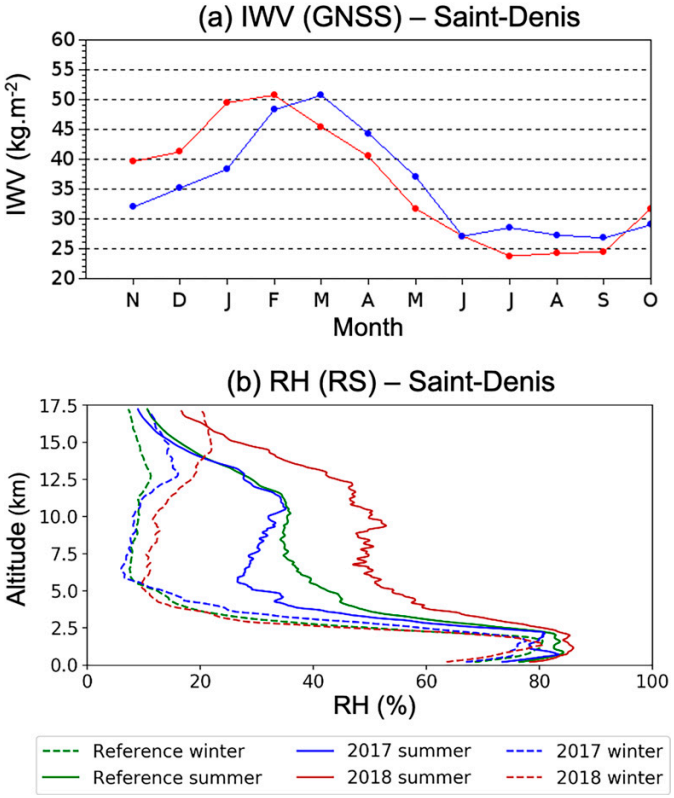

Figure 9. (**a**) Monthly mean of GNSS-derived IWV content at station REUN in 2017 (blue) and 2018 (red). (**b**) RS-derived relative humidity at Saint-Denis during summer (plain) and winter (dashed) 2017 (blue) and 2018 (red). The green line in (**b**) shows corresponding average RH profiles for the period 2014–2018.

According to seasonally averaged relative humidity data inferred from operational radio sounding observations in Saint-Denis (Figure 9b), absolute moisture conditions in summer 2018 (red solid line) were higher throughout the troposphere compared to summer 2017 (blue solid line), with an increase ranging from 10% at low levels to 100% at mid and high levels. The 5-y average (2014–2018) humidity profile (green solid line) also indicates that humidity conditions were significantly below (resp. above) normal in summer 2017 (resp. 2018), in good agreement with moisture anomaly patterns deduced from the analysis of ERA5 data (Figure 7g,h). In winter 2018, the seasonally averaged relative humidity profile (red dashed line) shows good agreement with the climatological mean (green dashed line) up to 6 km, and above normal relative humidity at higher levels. In 2017 (blue-dashed line), one can however observe a significant increase in the low-level relative humidity between 2 and 4 km altitude, ranging from +50% to +80% at a given level.

To further investigate relationships between cloudiness and humidity over Saint-Denis, Figure 10 shows hourly relative anomalies (difference between the hourly value and the daily average, divided by the daily average) of integrated water vapour (IWV, %), radar-derived low- (LLC, 1–3 km) and mid-to-high-level (HLC, 5–10 km) cloudiness (%) as well as insolation, during summer (left panel) and winter (right panel) 2018 (as GNSS

observations collocated with BASTA-REUNION only started to be available in January 2018, we can only compare cloud occurrence and IWV for this year).

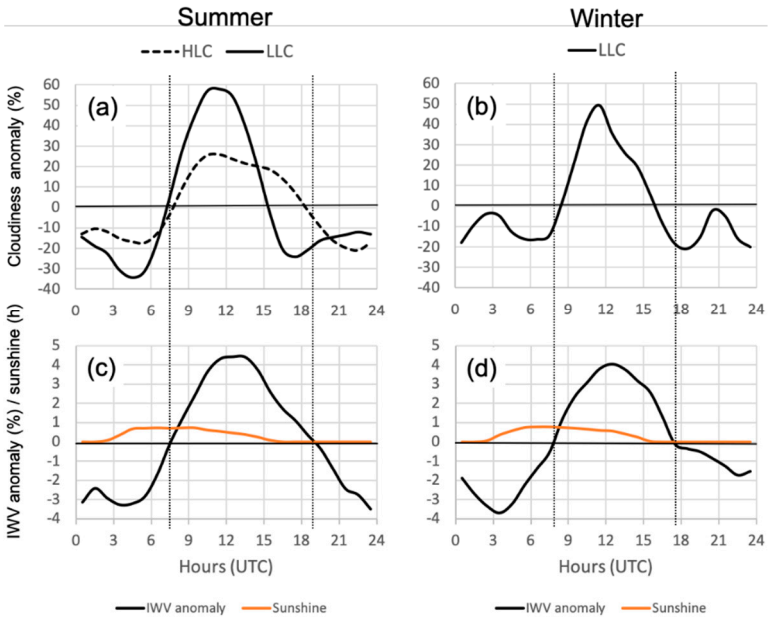

Figure 10. Diurnal cycle of high level (HLC) and low-level (LLC) clouds, Integrated water vapour (IWV) and insolation at Saint-Denis in 2018. Top panel: low-(1–3 km, plain) and mid-(5–10 km, dashed) level cloud anomaly (%) during (**a**) summer 2018 and (**b**) winter 2018. Bottom panel: Diurnal cycles of GNSS-derived (STDE station) IWV anomaly (%, black) and insolation (hours, orange) during (**c**) summer 2018 and (**d**) winter 2018.

The ground starts to heat up in the early morning (3 UTC/7 LST) with sunrise (Figure 10c,d), which increases the air temperature and initiates thermal instability in the boundary layer. As water vapour generated by evapotranspiration starts to condense, a positive cloudiness anomaly appears near 7:30 UTC (11:30 LST) at both low- and mid-to-high levels. A positive IWV anomaly, which remains positive throughout the daytime, can also be observed at nearly the same hour. In both summer (Figure 10c) and winter (Figure 10d) this positive moisture anomaly is maximum near 12 UTC (16 LST) and reaches about 4.5% (~2 kg m^{-2} in summer and 1.06 kg m^{-2} in winter). The time of this maximum likely reflects the existence of a sea breeze regime, which is strongest in mid-afternoon, when the difference in temperature between the land and ocean is highest. This IWV anomaly maximum also corresponds to that of the observed maximum in low-level cloudiness anomaly, which reaches up to 60% in summer (Figure 10a) and 50% in winter. This agreement suggests that the sea breeze regime may act to reinforce low-level cloud formation along the slopes through the advection of additional moisture originating from the ocean towards the island.

5. Discussion and Conclusions

The permanent deployment, in 2016, of a 95 GHz vertically pointing cloud radar BASTA in Reunion Island is an important achievement in order to reinforce cloud observations and atmospheric science research capabilities in the SWIO.

Data collected by this radar during its two first years of operation show a strong seasonal cycle with significant variation of cloudiness between summers and winters. During Austral summer, a bimodal mode characterized by two cloud layers extending respectively from 1–3 km (maximum daily frequency of cloud occurrence of 45%) and 8–12 km (maximum daily frequency of cloud occurrence of 15%) is observed. During Austral winter, cloudiness is mostly limited to the low levels (maximum daily probability of occurrence of about 35%) due to both the northward migration of the ITCZ and the

strong trade wind inversion prevailing at this time of the year (which further limits vertical cloud extension). These results are globally in line with those obtained by [19] over the tropical island of Barbados (using ground-based cloud radar data collected over a similar period of two years), which have also shown the existence of a bimodal mode (in the vertical) in summer that disappears in winter due to the circulation shifts accompanying the seasonal migration of the ITCZ. As in [19], we also observed a slight variability in the lower troposphere cloudiness across the seasons on a diurnal scale. In summer, medium and high clouds associated with convective developments over the island's relief show a maximum occurrence between 10 and 15UTC (i.e., between 14 and 19 LST), while low-level clouds are maximised between 8 and 15 UTC (12 and 19 LST) in summer and 9 and 14 UTC (13 and 18 LST) in winter. As in Barbados, this variability appears somewhat more important in summer (maximum value of cloud occurrence of 45% at a height of 2 km at both locations) than during winter (25% in Barbados vs. 35% in Reunion Island at a height of 2 km). The diurnal cycle of the cloudiness is also strongly correlated with the diurnal cycle of IWV regardless of the season and the cloud layer considered.

The comparative analysis of seasonal cloudiness observations collected in 2017 and 2018 also shows strong differences from one year to the next, with significantly higher (resp. lower) cloud cover in winter (resp. summer) 2017 than in 2018. The analysis of ERA5 reanalysis data and local humidity measurements derived from radio soundings and GNSS observations suggests that these differences could be attributed to a different large-scale context between the two years. In summer 2017 a strong positive SST anomaly, which formed in relationship with a positive phase of the subtropical Indian Ocean dipole (SIOD), could be observed south of Madagascar and was accompanied by positive (resp. negative) anomalies of subsidence (resp. humidity) over the center part of the basin. This large-scale subsidence, and associated dry air, acted to limit the vertical extension of clouds and likely explains the significant differences in cloud cover observed between the two summers. The two winter seasons also show important differences in terms of the large-scale environment. In 2017, a zonal dipole of large-scale subsidence anomaly was observed, while conditions were closer to normal in 2018. The eastward shift of high subsidence values resulting from the presence of this dipole resulted in a wet anomaly over the western part of the basin in winter 2017 that was further amplified by a positive SST anomaly over Reunion Island (increased evaporation). As a consequence, the vertical structure of the cloudiness and the probability of cloud occurrence in the lower half of the troposphere were surprisingly similar throughout the year 2017.

According to regional and local humidity data, one can hypothesize that the 2017 IOSD event significantly impacted moisture conditions over Reunion Island throughout the year 2017, resulting in lower (resp. higher) than normal humidity conditions at low- and mid-level in summer (resp. winter). These distinct moisture conditions may have accounted for the large differences observed in terms of cloudiness between Austral summers 2017 and 2018 (Figure 4). The thermodynamic structure of the atmosphere over Reunion Island was also more unstable during Austral winter 2017 than during Austral winter 2018, thus favouring low-level cloud development, which eventually happens to overshoot the trade wind inversion. In this regard, an exceptional and extremely intense storm, which locally produced more than 105 mm of rainfall in one hour in the northeast part of the island, occurred on 29 and 30 August 2017. BASTA-REUNION reflectivity measurements collected at Saint-Denis during this event (Figure 11) show convective cells with vertical development above 7 km altitude, which is extremely uncommon in this season. Instantaneous rainfall data collected next to the radar on 30 August around 1:30 LST confirms that particularly intense rainfall (up to 70 mmh^{-1}) occurred over Saint-Denis even though the rainfall maxima was observed about 15 km SE of the radar. Additionally, note the extinction of the radar signal at the same hour, as already observed in Figures 2 and 3.

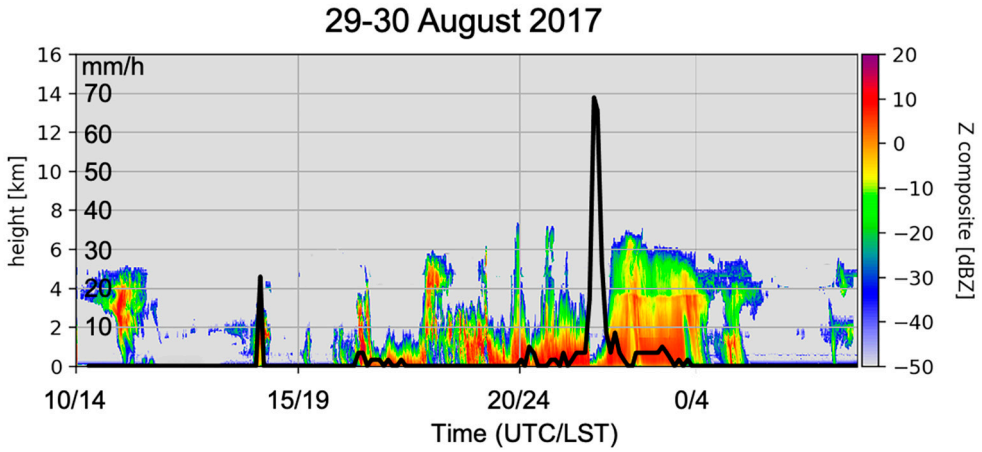

Figure 11. As in Figure 2, but for data collected between 29 August (10 UTC/14 LST) and 30 August (5 UTC/9 LST) 2017.

Decreased moisture at low levels during summer 2017 can also account for the limited development of deep local convective events with respect to 2018. The observed differences in terms of cloudiness were also exacerbated by the significant cyclonic activity that occurred over the Mascarene Archipelago during the wet season 2018. Between January and April 2018 (see Figure 1 in [38]), four tropical cyclones grazed the island (TC Berguitta and Fakir) or passed in its immediate vicinity (TC Ava and Dumazile)—which drained a large amount of mid-to-high level clouds over Reunion Island—whereas only two tropical storms (TS Carlos and Fernando), which passed more than 200 km away from the island, occurred in 2017.

Cloud radar observations are key to investigate the properties and variability of tropical clouds, to evaluate cloud fraction forecasted by NWP systems [39] and derived from space-borne measurements, as well as to evaluate climate model performance [40]. Although limited in time, the preliminary analysis of the 2-y dataset of cloud radar observations analysed in this study already allows us to better understand the various and complex processes that drive cloudiness in the tropical island of the SWIO such as Reunion Island. More efforts are nevertheless obviously needed in order to thoroughly characterize the properties of the clouds in this tropical area as well as to fully exploit the rare observations provided by research cloud radars in the Southern hemisphere.

In this regard, observations of clouds and precipitation in Reunion Island will continue to be reinforced in the frame of ACTRIS through the deployment, in late 2021, of a second, volumetric (i.e., 360° scanning), BASTA cloud radar at the Maïdo observatory. A transportable polarimetric X-band radar, aiming at complementing observations provided by Reunion Island's two operational S-band weather radar systems, will also be installed at Saint-Joseph (southern part of the island) in September 2021, in the frame of the Interreg-V Indian Ocean research project ESPOIRS ("Etude des Systèmes Precipitant de l'Océan Indien par Radars et Satellites" [41]). The deployment of this additional cloud radar, together with the enhancement of the ground-based weather radar network, will allow for further, long-term, studies of the seasonal and inter-annual variability of tropical clouds, but also to benefit from multi-frequency radar observations to better understand the formation and life cycle of clouds and precipitation over this unique tropical area. This new setup will thus permit us to study all sorts of cloud patterns, ranging from orographic, cirrus and low-to-mid level trade clouds to deep convective storms associated with tropical cyclones passing nearby. Altogether, these instruments will also contribute to make OPAR and Reunion Island a precious satellite validation testbed in the southern hemisphere for Earth observation programs, such as the upcoming EARTHCARE [42] space mission.

Author Contributions: Conceptualization J.D. (Jonathan Durand) and O.B.; data acquisition and processing J.D. (Julien Delanoë), J.D. (Jonathan Durand) and O.B.; writing—original draft preparation, J.D. (Jonathan Durand), E.L., F.B. and O.B.; writing—review and editing, all co-authors; supervision, O.B.; project administration, O.B.; funding acquisition, O.B. All authors have read and agreed to the published version of the manuscript.

Funding: This research was funded by the European Union, the Regional Council of Reunion Island and the French state under FEDER projects "BASTA-Reunion" and "ESIEC-RUN" and INTERREG-V Indian Ocean 2014–2020 project "ReNovRisk-Cyclone and Precipitation".

Institutional Review Board Statement: Not applicable.

Informed Consent Statement: Not applicable.

Data Availability Statement: Data used in this study are available on request from the corresponding author.

Acknowledgments: Authors are grateful to the engineers of the Laboratoire Atmosphère, Milieux et Observations Spatiales (LATMOS) for their help in the setup and operation of the BASTA-REUNION radar.

Conflicts of Interest: The authors declare no conflict of interest.

References

1. Liou, K.-N. Influence of Cirrus Clouds on Weather and Climate Processes: A Global Perspective. *Mon. Weather. Rev.* **1986**, *114*, 1167–1199. [CrossRef]
2. Hansen, J.; Sato, M.; Ruedy, R. Radiative forcing and climate response. *J. Geophys. Res. Space Phys.* **1997**, *102*, 6831–6864. [CrossRef]
3. Klein, S.A.; Hall, A.; Norris, J.R.; Pincus, R. Low-Cloud Feedbacks from Cloud-Controlling Factors: A Review. *Surv. Geophys.* **2017**, *38*, 1307–1329. [CrossRef]
4. Bony, S. Marine boundary layer clouds at the heart of tropical cloud feedback uncertainties in climate models. *Geophys. Res. Lett.* **2005**, *32*, 20806. [CrossRef]
5. Stephens, G.L. Cloud Feedbacks in the Climate System: A Critical Review. *J. Clim.* **2005**, *18*, 237–273. [CrossRef]
6. Nuijens, L.; Stevens, B.; Siebesma, A.P. The Environment of Precipitating Shallow Cumulus Convection. *J. Atmos. Sci.* **2009**, *66*, 1962–1979. [CrossRef]
7. Madden, R.; Julian, P. Detection of a 40-50-day oscillation of the zonal wind in the tropical Pacific. *J. Atmos. Sci.* **1971**, *28*, 702–708. [CrossRef]
8. Madden, R.; Julian, P. Observations of the 40–50-day tropical oscillation. A review. *Mon. Wea. Rev.* **1994**, *122*, 814–837. [CrossRef]
9. Battaglia, A.; Kollias, P.; Dhillon, R.; Lamer, K.; Khairoutdinov, M.; Watters, D. Mind the gap–Part 2: Improving quantitative estimates of cloud and rain water path in oceanic warm rain using spaceborne radars. *Atmos. Meas. Tech.* **2020**, *13*, 4865–4883. [CrossRef]
10. Marchand, R.; Mace, G.G.; Ackerman, T.; Stephens, G. Hydrometeor Detection Using Cloudsat—An Earth-Orbiting 94-GHz Cloud Radar. *J. Atmos. Ocean. Technol.* **2008**, *25*, 519–533. [CrossRef]
11. Sassen, K.; Wang, Z. Classifying clouds around the globe with the CloudSat radar: 1-year of results. *Geophys. Res. Lett.* **2008**, *35*, 04805. [CrossRef]
12. Lamer, K.; Kollias, P.; Battaglia, A.; Preval, S. Mind the gap–Part 1: Accurately locating warm marine boundary layer clouds and precipitation using spaceborne radars. *Atmos. Meas. Tech.* **2020**, *13*, 2363–2379. [CrossRef]
13. Kollias, P.; Clothiaux, E.E.; Miller, M.A.; Albrecht, B.A.; Stephens, G.L.; Ackerman, T.P. Millimeter-Wavelength Radars: New Frontier in Atmospheric Cloud and Precipitation Research. *Bull. Am. Meteorol. Soc.* **2007**, *88*, 1608–1624. [CrossRef]
14. Long, C.N.; Mather, J.H.; Ackerman, T.P. The ARM Tropical Western Pacific (TWP) Sites. *Meteorol. Monogr.* **2016**, *57*, 7. [CrossRef]
15. Thorsen, T.J.; Fu, Q.; Comstock, J. Cloud effects on radiative heating rate profiles over Darwin using ARM and A-train radar/lidar observations. *J. Geophys. Res. Atmos.* **2013**, *118*, 5637–5654. [CrossRef]
16. Liu, Z.; Marchand, R.; Ackerman, T. A comparison of observations in the tropical western Pacific from ground-based and satellite millimeter-wavelength cloud radars. *J. Geophys. Res. Space Phys.* **2010**, *115*. [CrossRef]
17. Bouniol, D.; Couvreux, F.; Kamsu-Tamo, P.; Leplay, M.; Guichard, F.; Favot, F.; O'Connor, E.J. Diurnal and Season-al Cycles of Cloud Occurrences, Types, and Radiative Impact over West Africa. *J. Appl. Meteorol. Clim.* **2012**, *51*, 534–553. [CrossRef]
18. Sukanya, P.; Kalapureddy, M.C.R. Cloud radar observations of multi-scale variability of cloud vertical structure associated with Indian summer monsoon over a tropical location. *Clim. Dyn.* **2021**, *56*, 1055–1081. [CrossRef]
19. Stevens, B.; Farrell, D.; Hirsch, L.; Jansen, F.; Nuijens, L.; Serikov, I.; Brügmann, B.; Forde, M.; Linné, H.; Lonitz, K.; et al. The Barbados Cloud Observatory: Anchoring Investigations of Clouds and Circulation on the Edge of the ITCZ. *Bull. Am. Meteorol. Soc.* **2016**, *97*, 787–801. [CrossRef]
20. Stevens, B.D.; Bony, S.; Farrell, D.; Ament, F. EUREC4A, submitted to Earth. *Sys. Sci. Data*. 2021. Available online: https://essd.copernicus.org/preprints/essd-2021-18/ (accessed on 29 May 2021).

21. Brueck, M.; Nuijens, L.; Stevens, B. On the Seasonal and Synoptic Time-Scale Variability of the North Atlantic Trade Wind Region and Its Low-Level Clouds. *J. Atmos. Sci.* **2015**, *72*, 1428–1446. [CrossRef]
22. Kollias, P.; Bharadwaj, N.; Clothiaux, E.E.; Lamer, K.; Oue, M.; Hardin, J.; Isom, B.; Lindenmaier, I.; Matthews, A.; Luke, E.; et al. The ARM Radar Network: At the Leading Edge of Cloud and Precipitation Observations. *Bull. Am. Meteorol. Soc.* **2020**, *101*, E588–E607. [CrossRef]
23. Baray, J.-L.; Courcoux, Y.; Keckhut, P.; Portafaix, T.; Tulet, P.; Cammas, J.-P.; Hauchecorne, A.; Godin Beekmann, S.; De Mazière, M.; Hermans, C.; et al. Maïdo observatory: A new high-altitude station facility at Reunion Island (21° S, 55° E) for long-term atmospheric remote sensing and in situ measurements. *Atmos. Meas. Tech.* **2013**, *6*, 2865–2877. [CrossRef]
24. Delanoë, J.; Protat, A.; Vinson, J.-P.; Brett, W.; Caudoux, C.; Bertrand, F.; Du Chatelet, J.P.; Hallali, R.; Barthes, L.; Haeffelin, M.; et al. BASTA: A 95-GHz FMCW Doppler Radar for Cloud and Fog Studies. *J. Atmos. Ocean. Technol.* **2016**, *33*, 1023–1038. [CrossRef]
25. Bergemann, M.; Jakob, C. How important is tropospheric humidity for coastal rainfall in the tropics? *Geophys. Res. Lett.* **2016**, *43*, 5860–5868. [CrossRef]
26. Dupont, J.-C.; Haeffelin, M.; Wærsted, E.; Delanoe, J.; Renard, J.-B.; Preissler, J.; O'Dowd, C. Evaluation of Fog and Low Stratus Cloud Microphysical Properties Derived from In Situ Sensor, Cloud Radar and SYRSOC Algorithm. *Atmosphere* **2018**, *9*, 169. [CrossRef]
27. Quetelard, H.; Bessemoulin, P.; Cerveny, R.S.; Peterson, T.C.; Burton, A.; Boodhoo, Y. Extreme Weather: World-Record Rainfalls During Tropical Cyclone Gamede. *Bull. Am. Meteorol. Soc.* **2009**, *90*, 603–608. [CrossRef]
28. Taupin, F.G.; Bessafi, M.; Baldy, S.; Bremaud, P.J. Tropospheric ozone above the southwestern Indian Ocean is strongly linked to dynamical conditions prevailing in the tropics. *J. Geophys. Res. Space Phys.* **1999**, *104*, 8057–8066. [CrossRef]
29. Brémaud, P.; Taupin, F. Cloud influence on ozone diurnal cycle in the marine boundary layer at Réunion Island. *Atmos. Res.* **1998**, *47–48*, 285–298. [CrossRef]
30. Lesouëf, D.; Gheusi, F.; Delmas, R.; Escobar, J. Numerical simulations of local circulations and pollution transport over Reunion Island. *Ann. Geophys.* **2011**, *29*, 53–69. [CrossRef]
31. Réchou, A.; Flores, O.; Jumaux, G.; Duflot, V.; Bousquet, O.; Pouppeville, C.; Bonnardot, F. Spatio-temporal variability of rainfall in a high tropical island: Patterns and large-scale drivers in Réunion Island. *Q. J. R. Meteorol. Soc.* **2019**, *145*, 893–909. [CrossRef]
32. Rechou, A.; Rao, T.N.; Bousquet, O.; Plu, M.; Decoupes, R. Properties of rainfall in a tropical volcanic island deduced from UHF wind profiler measurements. *Atmos. Meas. Tech.* **2014**, *7*, 409–418. [CrossRef]
33. Jumeaux, G.; Quetelard, H.; Roy, D. Atlas Climatique de La Réunion of Météo-France, Météo-France technical report 2011. (in French). Available online: http://www.meteofrance.fr/publications/nos-collections/climat-outre-mer/atlas-climatique-de-la-reunion (accessed on 29 May 2021).
34. Lees, E.; Bousquet, O.; Roy, D.; Leclair, J. Analysis of diurnal to seasonal variability of integrated water vapour in the South Indian Ocean basin using ground-based GNSS and 5th generation ECMWF reanalysis (ERA5) data. *Q. J. R. Meteorol.* **2021**, *147*, 229–248. [CrossRef]
35. Bousquet, O.; Lees, E.; Durand, J.; Peltier, A.; Duret, A.; Mekies, D.; Boissier, P.; Donal, T.; Fleischer-Dogley, F.; Zakariasy, L. Densification of the Ground-Based GNSS Observation Network in the Southwest Indian Ocean: Current Status, Perspectives, and Examples of Applications in Meteorology and Geodesy. *Front. Earth Sci.* **2020**, *8*. [CrossRef]
36. Hersbach, H.; Bell, B.; Berrisford, P.; Hirahara, S.; Horanyi, A.; Muñoz-Sabater, J.; Nicolas, J.; Peubey, C.; Radu, R.; Schepers, D.; et al. The ERA5 global reanalysis. *Q. J. R. Meteorol. Soc.* **2020**, *146*, 1999–2049. [CrossRef]
37. Behera, S.; Yamagata, T. Subtropical SST dipole events in the southern Indian Ocean. *Geophys. Res. Lett.* **2001**, *28*, 327–330. [CrossRef]
38. Bousquet, O.; Barbary, D.; Bielli, S.; Kebir, S.; Raynaud, L.; Malardel, S.; Faure, G. An evaluation of tropical cyclone forecast in the Southwest Indian Ocean basin with AROME-Indian Ocean convection-permitting numerical weather predicting system. *Atmos. Sci. Lett.* **2019**, *21*, 950. [CrossRef]
39. Hogan, R.J.; O'Connor, E.J.; Illingworth, A.J. Verification of cloud-fraction forecasts. *Q. J. R. Meteorol. Soc.* **2009**, *135*, 1494–1511. [CrossRef]
40. Protat, A.; Bouniol, D.; Delanoë, J.; May, P.T.; Plana-Fattori, A.; Hasson, A.; Görsdorf, U.; Heymsfield, A.J. As-sessment of Cloudsat Reflectivity Measurements and Ice Cloud Properties Using Ground-Based and Airborne Cloud Radar Observations. *J. Atmos. Ocean. Technol.* **2009**, *26*, 1717–1741. [CrossRef]
41. Bousquet, O.; Barruol, G.; Cordier, E.; Barthe, C.; Bielli, S.; Calmer, R.; Rindraharisaona, E.; Roberts, G.; Tulet, P.; Amelie, V.; et al. Impact of Tropical Cyclones on Inhabited Areas of the SWIO Basin at Present and Future Horizons. Part 1: Overview and Observing Component of the Research Project RENOVRISK-CYCLONE. *Atmosphere* **2021**, *12*, 544. [CrossRef]
42. Illingworth, A.J.; Barker, H.W.; Beljaars, A.; Ceccaldi, M.; Chepfer, H.; Clerbaux, N.; Cole, J.; Delanoë, J.; Domènech, C.; Donovan, D.P.; et al. The EarthCARE Satellite: The Next Step Forward in Global Measurements of Clouds, Aerosols, Precipitation, and Radiation. *Bull. Am. Meteorol. Soc.* **2015**, *96*, 1311–1332. [CrossRef]